nature physics

Article https://doi.org/10.1038/s41567-024-02384-5

Phonon chirality from impurity scattering in the antiferromagnetic phase of Sr_2IrO_4

Received: 7 February 2023

Accepted: 19 December 2023

Published online: 30 January 2024

Check for updates

A. Ataei [1] ✉, G. Grissonnanche [1,2], M.-E. Boulanger [1], L. Chen [1], É. Lefrançois [1], V. Brouet [3] & L. Taillefer [1,4] ✉

A thermal Hall effect occurs in an increasing number of insulators and is often attributed to phonons, but the underlying mechanism is not known in most cases. Two main scenarios have been proposed: either a coupling of phonons to spins or scattering of phonons by impurities or defects, but there is no systematic evidence to support either of them. Here we present evidence for the phonon impurity scattering picture by studying the effect of adding rhodium impurities to the antiferromagnetic insulator Sr_2IrO_4, substituting for the spin-carrying iridium atoms. We find that adding small concentrations of rhodium impurities increases the thermal Hall conductivity, but adding enough rhodium to suppress the magnetic order eventually decreases it until it nearly vanishes. In contrast, introducing lanthanum impurities that substitute for the strontium atoms, which lie outside the IrO_2 planes that are the seat of magnetism, produces a much smaller enhancement of the thermal Hall conductivity. We conclude that the thermal Hall effect in this material is caused by the scattering of phonons by impurities embedded within a magnetic environment.

The thermal Hall effect is used increasingly to probe insulators[1–11], materials with no mobile charge carriers. In the presence of a heat current J along the x axis and a magnetic field H along the z axis, a transverse temperature gradient ∇T (along the y axis) can develop even if the carriers of heat are chargeless, provided they have chirality[12] or they acquire a handedness in the presence of a magnetic field. Of particular interest is the possibility that measurements of the thermal Hall conductivity κ_{xy} could detect emergent excitations in quantum materials, such as Majorana fermions[13] or chiral magnons[14], reportedly sighted in the spin liquid candidate α-$RuCl_3$ (refs. 15,16, although some authors have a different interpretation[10,17]).

Phonons are the dominant carriers of heat in all insulators, and so the first question to ask of any thermal Hall study is whether phonons are responsible for κ_{xy}. Initially, they were thought to generate only a very small thermal Hall effect, but we now know, for example, from observations in multiferroic materials[8], cuprate Mott insulators[9,18], strontium titanate[6] and the antiferromagnetic insulator Cu_3TeO_6 (ref. 11), that this is not true. However, although it is now clear that phonons can produce a sizeable thermal Hall signal, the underlying microscopic mechanism is still not clear. Several theoretical scenarios have been proposed in the last few years[19–28], most recently focusing on the role played by impurity or defect scattering of phonons[24–26,28]. Of particular interest here is a mechanism of resonant scattering of phonons by defects embedded in an antiferromagnetic environment, which does generate a thermal Hall effect of a realistic magnitude[28].

In this Article, we report a systematic study of how Rh impurities affect the thermal Hall conductivity of the antiferromagnetic insulator Sr_2IrO_4. Despite the fact that Rh is isovalent to Ir, X-ray absorption experiments[29] have shown that, at small dopings, Rh adopts a valence 3+, with a non-magnetic $4d^6$ configuration, different from the $5d^5$ configuration of Ir^{4+}. Hence, it acts as a non-magnetic impurity, effectively trapping an electron and therefore doping the rest of the system with holes, as confirmed by angle-resolved photoemission experiments[30,31]. Magnetism is progressively suppressed, and the system

[1]Institut quantique, Département de physique and RQMP, Université de Sherbrooke, Sherbrooke, Quebec, Canada. [2]Laboratoire des Solides Irradiés, CEA/DRF/lRAMIS, CNRS, École Polytechnique, Institut Polytechnique de Paris, Palaiseau, France. [3]Laboratoire de Physique des Solides, Université Paris-Saclay, CNRS, Orsay, France. [4]Canadian Institute for Advanced Research, Toronto, Ontario, Canada. ✉e-mail: amirreza.ataei@usherbrooke.ca; louis.taillefer@usherbrooke.ca

https://doi.org/10.1038/s41567-024-02384-5

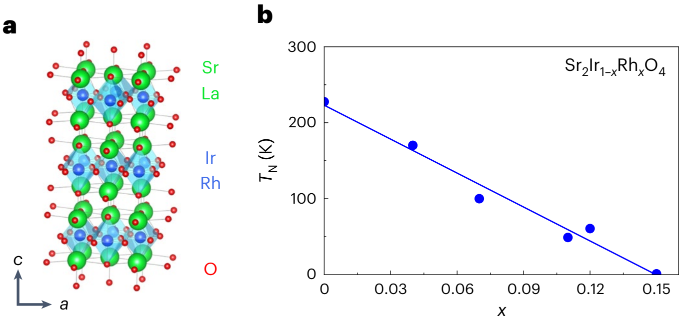

Fig. 1 | Crystal structure and magnetic phase diagram of Rh-doped Sr_2IrO_4. **a**, The crystal structure of Sr_2IrO_4, showing the stacking of IrO_2 layers. The spins (moments) reside on the Ir sites, and order into a Néel antiferromagnetic state at low temperature. Rh impurities substitute for the Ir atoms and La impurities substitute for the Sr atoms, on atomic sites as colour coded. The directions of the crystallographic axes *a* and *c* are indicated by arrows. **b**, The temperature–doping phase diagram of Sr_2IrO_4, showing how the antiferromagnetic transition temperature T_N (blue dots) decreases with Rh doping[30].

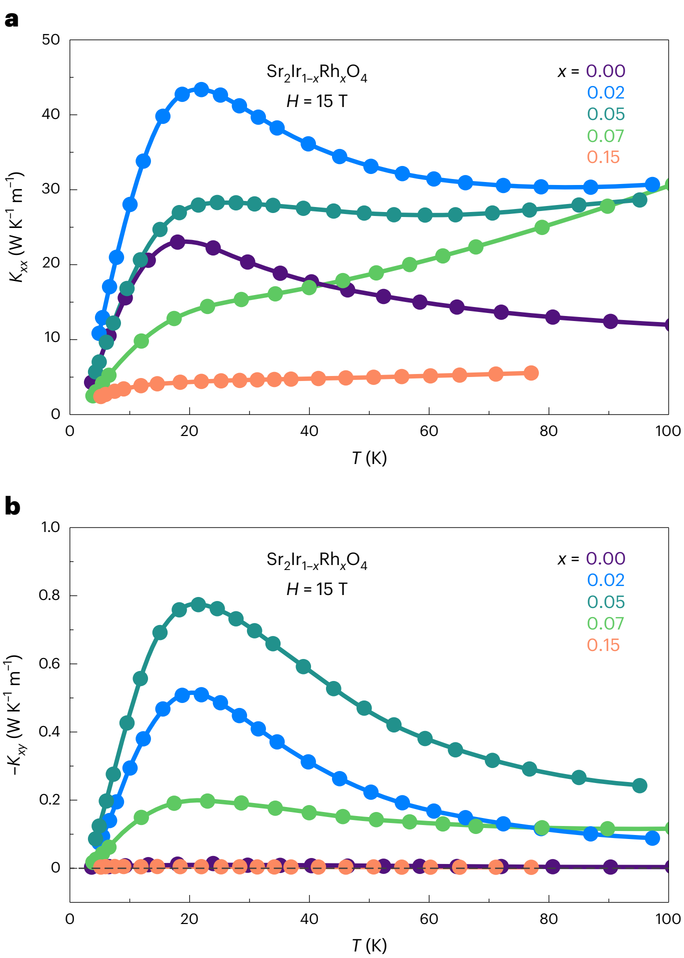

Fig. 2 | Thermal conductivity and thermal Hall conductivity in Rh-doped Sr_2IrO_4. **a**, The thermal conductivity κ_{xx} of $Sr_2Ir_{1-x}Rh_xO_4$ for a heat current parallel to the IrO_2 planes ($J \parallel a \parallel x$) and a magnetic field of 15 T applied normal to the planes ($H \parallel c \parallel z$), plotted as κ_{xx} versus T, for $x = 0$ (violet), $x = 0.02$ (blue), $x = 0.05$ (dark green), $x = 0.07$ (light green) and $x = 0.15$ (orange). **b**, The thermal Hall conductivity κ_{xy} for the same five samples, plotted as $-\kappa_{xy}$ versus T (κ_{xy} is negative for all samples at all temperatures). Data at different fields are shown in Extended Data Fig. 3, for $x = 0.05$.

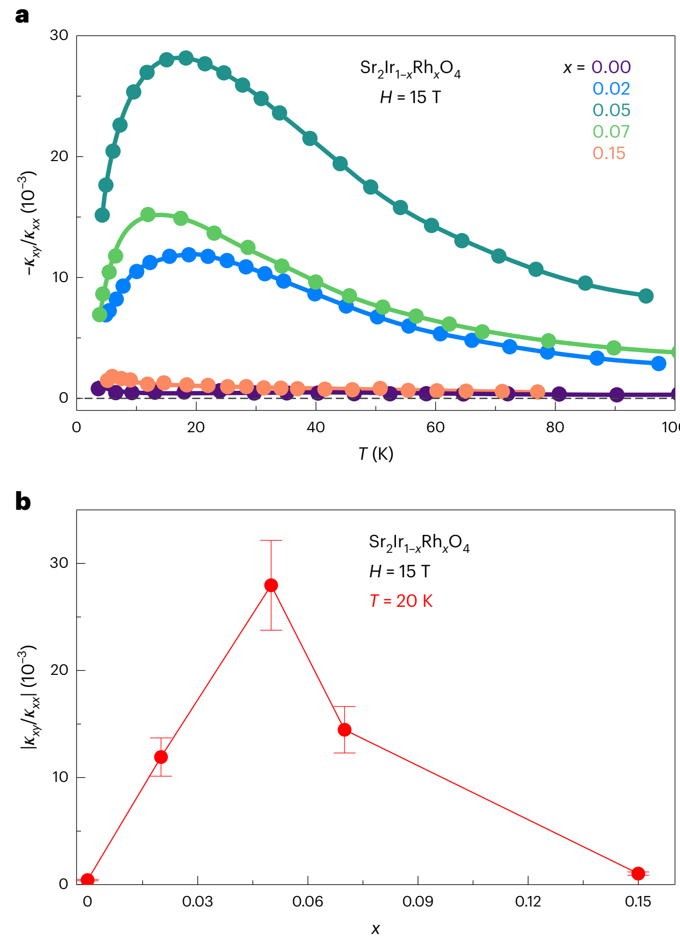

Fig. 3 | Thermal Hall angle as a function of Rh doping. **a**, The thermal Hall angle in our five samples of $Sr_2Ir_{1-x}Rh_xO_4$, plotted as $|\kappa_{xy}/\kappa_{xx}|$ versus T, obtained from κ_{xx} and κ_{xy} data in Fig. 2. **b**, The magnitude of $|\kappa_{xy}/\kappa_{xx}|$, at $T = 20$ K, as a function of the Rh doping. Note the 70-fold increase in $|\kappa_{xy}/\kappa_{xx}|$ between $x = 0$ and $x = 0.05$, and the subsequent decrease to a very small value at $x = 0.15$, where antiferromagnetic order has been suppressed (Fig. 1b). Error bars are ±15% (Methods).

becomes increasingly metallic[32]. We find that 2% of Rh substituting for the spin-carrying Ir atoms (Fig. 1a) causes a 30-fold enhancement of the thermal Hall angle, $|\kappa_{xy}/\kappa_{xx}|$, while 15% of Rh, enough to suppress the magnetic order (Fig. 1b), brings this down to a negligible value. We conclude that both impurities and magnetism play a key role.

Figure 2 and Extended Data Fig. 1 show our data for the thermal conductivity κ_{xx} and the thermal Hall conductivity κ_{xy}, taken at a magnetic field of 15 T on five samples of $Sr_2Ir_{1-x}Rh_xO_4$. These samples have Rh concentrations ranging from $x = 0$ to $x = 0.15$, and their doping concentrations were validated using energy dispersive X-ray spectroscopy (Extended Data Fig. 2). Extended Data Fig. 3 shows the typical field dependence of κ_{xx} and κ_{xy}. However, for all other thermal measurements, the applied magnetic field was maintained at 15 T. We see that small concentrations of Rh, up to $x = 0.05$, yield only small variations in the magnitude of κ_{xx} (Fig. 2a), no more than the factor of 2–3 variation that is typical of the sample-to-sample variation seen in oxide crystals (see, for example, ref. 33). Our κ_{xx} data at $x = 0$ are similar to those previously reported for Sr_2IrO_4 (ref. 34). We attribute the difference in amplitude to a difference in crystalline (structural) quality. By contrast, the same small concentrations of Rh cause a huge increase in the magnitude of κ_{xy} (Fig. 2b). Plotting the ratio $|\kappa_{xy}/\kappa_{xx}|$ versus T (Fig. 3a), we see that the peak value, at $T \approx 20$ K, increases very rapidly with x, at low x (Fig. 3b). Specifically, $|\kappa_{xy}/\kappa_{xx}|$ is 30 times larger at $x = 0.02$ compared with $x = 0$, and 70 times at $x = 0.05$. This is compelling

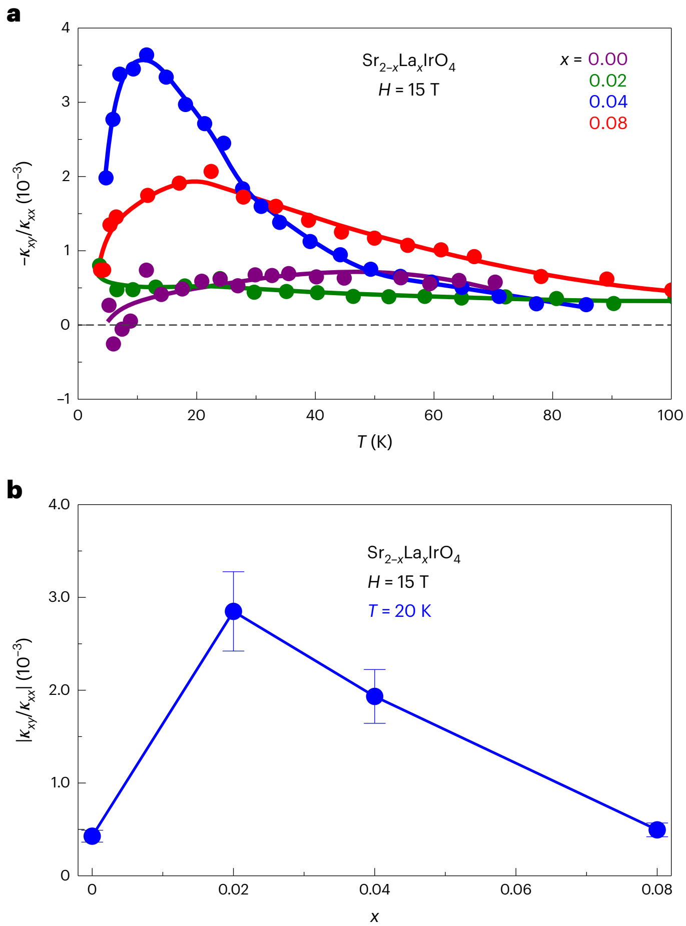

Fig. 4 | Thermal Hall angle as a function of La doping. **a**, The thermal Hall angle in our four samples of $\mathrm{Sr_{2-x}La_xIrO_4}$, plotted as $|\kappa_{xy}/\kappa_{xx}|$ versus T, obtained from κ_{xx} and κ_{xy} data in Extended Data Fig. 4. **b**, The magnitude of $|\kappa_{xy}/\kappa_{xx}|$, at $T = 20$ K, as a function of La doping. Note the six-fold increase in $|\kappa_{xy}/\kappa_{xx}|$ between $x = 0$ and $x = 0.02$, and the subsequent decrease as magnetic order is being suppressed. Error bars are ±15% (Methods).

evidence that impurity scattering plays a key role in the mechanism responsible for the thermal Hall effect in this insulator.

The heat carriers at play in $\mathrm{Sr_2IrO_4}$ are almost certainly phonons, given the similarity of $\kappa_{xy}(T)$ to findings for the cuprate Mott insulators $\mathrm{La_2CuO_4}$, $\mathrm{Nd_2CuO_4}$ and $\mathrm{Sr_2CuO_2Cl_2}$ (ref. 18), materials in which phonons have been shown to cause κ_{xy} (refs. 9,33). Specifically, $|\kappa_{xy}(T)|$ peaks at the same temperature ($T \approx 20$ K) as the phonon-dominated $\kappa_{xx}(T)$, as in the cuprates, and indeed $\mathrm{SrTiO_3}$ (ref. 6) and $\mathrm{Cu_3TeO_6}$ (ref. 11), materials where phonons are also clearly the relevant heat carriers.

The heat carriers at $T = 20$ K, where κ_{xy} is largest, are certainly not magnons because the gap in the magnon spectrum ensures that, at such a temperature, the contribution of magnons to heat transport is negligible[34]. Note also that charge carriers doped into the $\mathrm{IrO_2}$ planes when Rh is added make a negligible contribution to κ_{xx} and κ_{xy}, because of the very large electrical resistivity of our samples (Methods).

Our first major finding is therefore that impurity scattering plays a strong role in controlling the phonon thermal Hall effect in this material. We confirm this by introducing another type of impurity: La substituting for Sr. Figure 4 and Extended Data Fig. 4 report our data for four crystals of $\mathrm{Sr_{2-x}La_xIrO_4}$ with La concentrations ranging from $x = 0$ to $x = 0.08$. (La doping in excess of $x = 0.10$ suppresses antiferromagnetic order[35].) We see that adding low levels of La impurities again causes an increase in $|\kappa_{xy}/\kappa_{xx}|$ (Fig. 4a), but the effect is much less pronounced than for Rh doping (Extended Data Fig. 5). Indeed, when measured at $T = 20$ K (and $H = 15$ T), $|\kappa_{xy}/\kappa_{xx}|$ reaches a maximal value that is ten times smaller for La doping (Fig. 4b) compared with Rh doping (Fig. 3b). We infer that what matters is disorder on the spin-carrying site (Ir). In other words, spin also plays a key role.

We find further support for this inference by looking at higher doping levels. In Fig. 2b, we see that, when enough Rh is added to fully suppress the long-range antiferromagnetic order, namely $x = 0.15$ (so that the Néel temperature goes to zero; Fig. 1b), the magnitude of κ_{xy} becomes very small and $|\kappa_{xy}/\kappa_{xx}|$ is back down to its low value at $x = 0$ (Fig. 3b). A similar decrease of $|\kappa_{xy}/\kappa_{xx}|$ at high x is found for La doping (Fig. 4b). This strongly suggests that magnetism is a key ingredient. This is our second major finding.

In summary, our doping studies of the antiferromagnetic insulator $\mathrm{Sr_2IrO_4}$ show that impurities can generate a large phonon thermal Hall effect, especially when these impurities are embedded in a magnetic environment. This goes along the lines of a recent theoretical proposal based on resonant impurity scattering of phonons in a magnetic insulator[28]. A scenario of phonons scattered by impurities in a magnetic environment may be relevant for the thermal Hall effect of several other materials, such as the cuprates[5,9,18,33], whose magnetic order and crystal structure are very similar to those of $\mathrm{Sr_2IrO_4}$, but also the cubic antiferromagnet $\mathrm{Cu_3TeO_6}$ (ref. 11) and possibly spin liquid candidates such as the layered antiferromagnet α-$\mathrm{RuCl_3}$ (refs. 10,15,16).

Note that, unlike in $\mathrm{Sr_2IrO_4}$, the phonon thermal Hall angle in cuprates does not depend strongly on doping, whether this is hole doping (as in $\mathrm{La_2CuO_4}$ (ref. 5)) or electron doping (as in $\mathrm{Nd_2CuO_4}$ (ref. 33)). It is important to note, however, that unlike in Rh-doped $\mathrm{Sr_2IrO_4}$, the doping in cuprates proceeds via impurities (Sr in $\mathrm{La_2CuO_4}$ or Ce in $\mathrm{Nd_2CuO_4}$) that do not substitute for the spin-carrying site (Ir in $\mathrm{Sr_2IrO_4}$ and Cu in $\mathrm{La_2CuO_4}$ or $\mathrm{Nd_2CuO_4}$). The phonon thermal Hall effect in cuprates exists even outside the region of long-range antiferromagnetic order but is only observed in the doping range below p^*, the pseudogap critical point in hole-doped cuprates[5,9], and below $x^* = 0.175$, the critical doping below which short-range antiferromagnetic order is known to exist in electron-doped cuprates[33]. It therefore seems that short-range magnetic correlations are also important for the phonon thermal Hall effect of cuprates, with the implication that such correlations are a defining characteristic of the pseudogap phase.

Online content

Any methods, additional references, Nature Portfolio reporting summaries, source data, extended data, supplementary information, acknowledgements, peer review information; details of author contributions and competing interests; and statements of data and code availability are available at https://doi.org/10.1038/s41567-024-02384-5.

References

1. Strohm, C., Rikken, G. L. J. A. & Wyder, P. Phenomenological evidence for the phonon Hall effect. *Phys. Rev. Lett.* **95**, 155901 (2005).
2. Onose, M. et al. Observation of the magnon Hall effect. *Science* **329**, 297–299 (2010).
3. Katsura, H., Nagaosa, N. & Lee, P. A. Theory of the thermal Hall effect in quantum magnets. *Phys. Rev. Lett.* **104**, 066403 (2010).
4. Hirschberger, M. et al. Large thermal Hall conductivity of neutral spin excitations in a frustrated quantum magnet. *Science* **348**, 106–109 (2015).
5. Grissonnanche, G. et al. Giant thermal Hall conductivity in the pseudogap phase of cuprate superconductors. *Nature* **571**, 376–380 (2019).
6. Li, X. et al. Phonon thermal Hall effect in strontium titanate. *Phys. Rev. Lett.* **124**, 105901 (2020).
7. Li, X. et al. The phonon thermal Hall angle in black phosphorus. *Nat. Commun.* **14**, 1027 (2023).

8. Ideue, T. et al. Giant thermal Hall effect in multiferroics. *Nat. Mat.* **16**, 797–802 (2017).
9. Grissonnanche, G. et al. Chiral phonons in the pseudogap phase of cuprates. *Nat. Phys.* **16**, 1108–1111 (2020).
10. Lefrançois, É. et al. Evidence of a phonon Hall effect in the Kitaev spin liquid candidate α-$RuCl_3$. *Phys. Rev. X* **12**, 021025 (2022).
11. Chen, L. et al. Large phonon thermal Hall conductivity in the antiferromagnetic insulator Cu_3TeO_6. *Proc. Natl Acad. Sci. USA* **119**, e2208016119 (2022).
12. Lee, H., Han, J. H. & Lee, P. A. Thermal Hall effect of spins in a paramagnet. *Phys. Rev. B* **91**, 125413 (2015).
13. Nasu, J., Yoshitake, J. & Motome, Y. Thermal transport in the Kitaev model. *Phys. Rev. Lett.* **119**, 127204 (2017).
14. Zhang, E. Z., Chern, L. E. & Kim, Y.-B. Topological magnons for thermal Hall transport in frustrated magnets with bond-dependent interactions. *Phys. Rev. B* **103**, 174402 (2021).
15. Kasahara, Y. et al. Majorana quantization and half-integer thermal quantum Hall effect in a Kitaev spin liquid. *Nature* **559**, 227–231 (2018).
16. Czajka, P. et al. The planar thermal Hall conductivity in the Kitaev magnet α-$RuCl_3$. *Nat. Mater.* **22**, 36–41 (2023).
17. Czajka, P. et al. Oscillations of the thermal conductivity in the spin-liquid state of α-$RuCl_3$. *Nat. Phys.* **17**, 915–919 (2021).
18. Boulanger, M.-E. et al. Thermal Hall conductivity in the cuprate Mott insulators Nd_2CuO_4 and $Sr_2CuO_2Cl_2$. *Nat. Commun.* **11**, 5325 (2020).
19. Chen, J.-Y., Kivelson, S. A. & Sun, X.-Q. Enhanced thermal Hall effect in nearly ferroelectric insulators. *Phys. Rev. Lett.* **124**, 167601 (2020).
20. Samajdar, R. et al. Thermal Hall effect in square-lattice spin liquids: a Schwinger boson mean-field study. *Phys. Rev. B* **99**, 165126 (2019).
21. Ye, M. et al. Phonon Hall viscosity in magnetic insulators. Preprint at https://arxiv.org/abs/2103.04223 (2021).
22. Zhang, Y. et al. Phonon Hall viscosity from phonon-spinon interactions. *Phys. Rev. B* **104**, 035103 (2021).
23. Mangeolle, L., Balents, L. & Savary, L. Phonon thermal Hall conductivity from scattering with collective fluctuations. *Phys. Rev. X* **12**, 041031 (2022).
24. Flebus, B. & MacDonald, A. H. Charged defects and phonon Hall effects in ionic crystals. *Phys. Rev. B* **105**, L220301 (2022).
25. Guo, H. & Sachdev, S. Extrinsic phonon thermal Hall transport from Hall viscosity. *Phys. Rev. B* **103**, 205115 (2021).
26. Sun, X.-Q., Chen, J.-Y. & Kivelson, S. A. Large extrinsic phonon thermal Hall effect from resonant scattering. *Phys. Rev. B* **106**, 144111 (2022).
27. Varma, C. M. Thermal Hall effect in the pseudogap phase of cuprates. *Phys. Rev. B* **102**, 075113 (2020).
28. Guo, H., Joshi, D. G. & Sachdev, S. Resonant side-jump thermal Hall effect of phonons coupled to dynamical defects. *Proc. Natl Acad. Sci. USA* **119**, e2215141119 (2022).
29. Clancy, J. P. et al. Dilute magnetism and spin-orbital percolation effects in $Sr_2Ir_{1-x}Rh_xO_4$. *Phys. Rev. B* **89**, 054409 (2014).
30. Louat, A. et al. Formation of an incoherent metallic state in Rh-doped Sr_2IrO_4. *Phys. Rev. B* **97**, 161109(R) (2018).
31. Cao, Y. et al. Hallmarks of the Mott-metal crossover in the hole-doped pseudospin-1/2 Mott insulator Sr_2IrO_4. *Nat. Commun.* **7**, 11367 (2016).
32. Qi, T. F. et al. Spin-orbit tuned metal-insulator transitions in single-crystal $Sr_2Ir_{1-x}Rh_xO_4$ ($0<x<1$). *Phys. Rev. B* **86**, 125105 (2012).
33. Boulanger, M.-E. et al. Thermal Hall conductivity of electron-doped cuprates. *Phys. Rev. B* **105**, 115101 (2022).
34. Steckel, F. et al. Pseudospin transport in the $J_{\mathrm{eff}}=1/2$ antiferromagnet Sr_2IrO_4. *Europhys. Lett.* **114**, 57007 (2016).
35. Gretarsson, H. et al. Persistent paramagnons deep in the metallic phase of $Sr_{2-x}La_xIrO_4$. *Phys. Rev. Lett.* **117**, 107001 (2016).

Publisher's note Springer Nature remains neutral with regard to jurisdictional claims in published maps and institutional affiliations.

Methods

Samples

Sr_2IrO_4 and Rh-doped Sr_2IrO_4. Single crystals of Sr_2IrO_4 and $Sr_2Ir_{1-x}Rh_xO_4$ were grown at Université Paris-Saclay using a flux-grown technique[36], with Rh concentrations of $x = 0.02$, 0.05, 0.07 and 0.15. Contacts were made using silver paste and thin silver wires.

La-doped Sr_2IrO_4. Single crystals of $Sr_{2-x}La_xIrO_4$ were also grown at Université Paris-Saclay with the same flux-grown technique, with La concentrations of $x = 0.02$, 0.04 and 0.08. Contacts were made in the same way.

The Rh and La content of the crystals was confirmed by EDX measurements (Extended Data Fig. 2). The orientation of the crystals is dictated by the rectangular shape of the as-grown platelets, as confirmed by several angle-resolved photoemission spectroscopy measurements on crystals grown in the same way.

Thermal Hall measurement

Thermal conductivity and thermal Hall conductivity measurements were performed as described in ref. 9. The thermal conductivity is defined as $\kappa_{xx} = (J/\Delta T_x)(l/wt)$, and the thermal Hall conductivity is defined as $\kappa_{xy} = -\kappa_{yy}(\Delta T_y/\Delta T_x)(l/w)$, where $\kappa_{yy} = \kappa_{xx}$ in this material given its tetragonal crystal structure and ΔT_y and ΔT_x are the transverse and longitudinal temperature differences across the sample, l is the distance between the longitudinal contacts, w and t are the sample width and thickness, respectively, and J is the heat current. The error bar on the absolute value of κ_{xy} is roughly ±25%, coming mostly from uncertainties in the values of l, w and t. As seen from the formulae above, the ratio κ_{xy}/κ_{xx} has a smaller error bar, roughly ±15%.

In all measurements, the heat current J was applied within the IrO_2 planes ($J \,||\, a$) and the magnetic field H was applied normal to the IrO_2 planes ($H \,||\, c$).

Electronic thermal Hall conductivity

Adding Rh to Sr_2IrO_4 introduces electronic charge carriers that themselves contribute to thermal transport, in both κ_{xx} and κ_{xy}. However, this contribution is negligible because all our Rh-doped samples have in-plane electrical resistivity $\rho_{xx} > 0.6$ mΩ cm below 100 K (ref. 30). Indeed, in our sample with $x = 0.15$, where the electrical Hall conductivity σ_{xy} is largest (being the most metallic), its value is such that $L_0\sigma_{xy} = 3$ μW K^{-2} m^{-1} for $H = 15$ T at $T = 20$ K (refs. 30,37), only 1% of the measured value of κ_{xy}/T for $H = 15$ T at $T = 20$ K. This negligible electronic contribution to κ_{xy} becomes even smaller for $x < 0.15$.

Reproducibility of our findings

In Extended Data Fig. 5a, we see that three separate samples of Rh-doped Sr_2IrO_4 with $x = 0.02$, 0.05 and 0.07 demonstrate the main conclusion of our paper, namely that a low level of Rh impurities causes a huge enhancement of the thermal Hall angle, by a factor of at least 30 relative to $x = 0$. We also see that three separate samples of La-doped Sr_2IrO_4 with $x = 0.02$, 0.04 and 0.08 demonstrate the second major conclusion of our paper, namely that La impurities cause a much smaller enhancement, by at least an order of magnitude compared with Rh doping. Having three separate samples that support each claim is a satisfactory level of reproducibility.

Moreover, the same level of reproducibility is observed if we look just at the thermal Hall conductivity itself, instead of the ratio κ_{xy}/κ_{xx}. This is immediately clear from Extended Data Fig. 5b, where we see that the raw κ_{xy} values for $x = 0.02$, 0.05 and 0.07 are at least a factor of 20 larger than at $x = 0$.

Factors of 30 and 20 are well beyond the expected variation from sample to sample.

Data availability

Source data are available with this paper. All other data that support the findings of this study are available from the corresponding authors upon reasonable request. Source data are provided with this paper.

References

36. Brouet, V. et al. Transfer of spectral weight across the gap of Sr_2IrO_4 induced by La doping. *Phys. Rev. B* **92**, 081117(R) (2015).
37. Fruchter, L. & Brouet, V. The 'dark phase' in $Sr_2Ir_{1-x}Rh_xO_4$ revealed by Seebeck and Hall measurements. *J. Phys. Condens. Matter* **33**, 215602 (2021).

Acknowledgements

We thank K. Behnia, H. Guo, D. Hsieh, S. A. Kivelson and S. Sachdev for fruitful discussions. L.T. acknowledges support from the Canadian Institute for Advanced Research (CIFAR) as a Fellow and funding from the Natural Sciences and Engineering Research Council of Canada (NSERC; PIN: 123817), the Fonds de recherche du Québec – Nature et Technologies (FRQNT), the Canada Foundation for Innovation (CFI) and a Canada Research Chair. This research was undertaken thanks in part to funding from the Canada First Research Excellence Fund. A.A. acknowledges support from the NSERC-CREATE programme QSciTech and Bourse d'excellence de l'Institut quantique à l'Université de Sherbrooke.

Author contributions

A.A., G.G., M.-E.B., L.C. and É.L. performed the thermal Hall conductivity measurements. A.A. prepared and characterized the samples. V.B. grew the single crystals of Sr_2IrO_4, $Sr_2Ir_{1-x}Rh_xO_4$ and $Sr_{2-x}La_xIrO_4$. A.A. and L.T. wrote the paper, in consultation with all authors. L.T. supervised the project.

Competing interests

The authors declare no competing interests.

Additional information

Extended data is available for this paper at https://doi.org/10.1038/s41567-024-02384-5.

Supplementary information The online version contains supplementary material available at https://doi.org/10.1038/s41567-024-02384-5.

Correspondence and requests for materials should be addressed to A. Ataei or L. Taillefer.

Peer review information *Nature Physics* thanks Andriy Nevidomskyy, and the other, anonymous, reviewers for their contribution to the peer review of this work.

https://doi.org/10.1038/s41567-024-02384-5

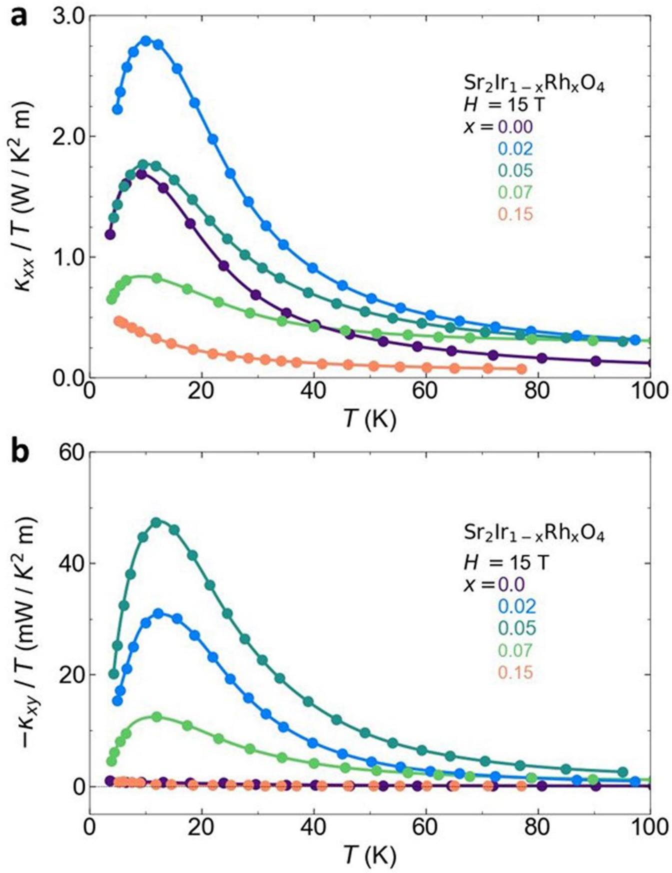

Extended Data Fig. 1 | Thermal conductivities in Rh-doped Sr_2IrO_4.
a) Thermal conductivity of $Sr_2Ir_{1-x}Rh_xO_4$ for a heat current parallel to the IrO_2 planes (J // a // x) and a magnetic field of 15 T applied normal to the planes (H // c // z), plotted as κ_{xx}/T vs T, for dopings x as indicated. **b)** Thermal Hall conductivity for the same samples, plotted as $-\kappa_{xy}/T$ vs T (κ_{xy} is negative in all samples at all temperatures).

https://doi.org/10.1038/s41567-024-02384-5

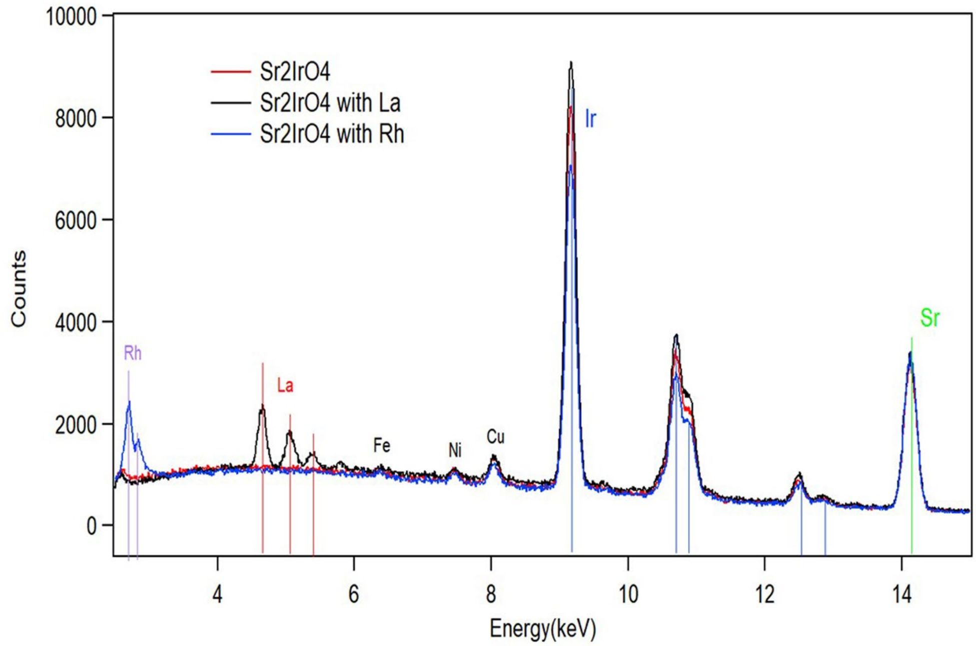

Extended Data Fig. 2 | EDX spectra of Sr_2IrO_4 samples. Typical EDX spectra for Sr_2IrO_4 (red), La-doped Sr_2IrO_4 (black) and Rh-doped Sr_2IrO_4 (blue). From such spectra taken on samples from the same batch as our transport samples, the value of x is confirmed, within an uncertainty of at most ± 20 %.

https://doi.org/10.1038/s41567-024-02384-5

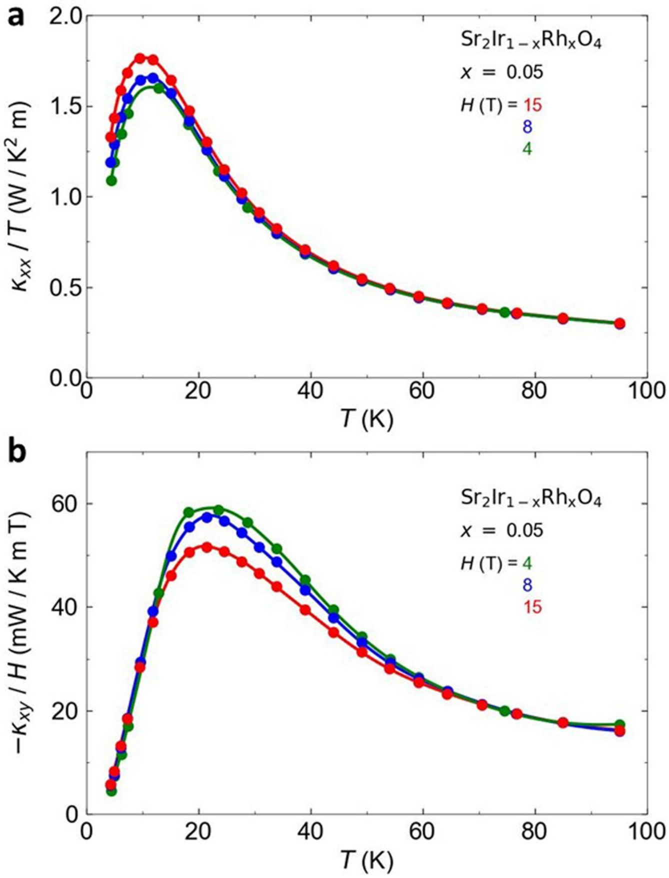

Extended Data Fig. 3 | Magnetic field dependence of κ_{xx} and κ_{xy}. a) Thermal conductivity of Rh-doped Sr_2IrO_4 with $x = 0.05$, plotted as κ_{xx}/T vs T for different magnetic fields, as indicated. **b)** Thermal Hall conductivity of the same sample, plotted as $-\kappa_{xy}/H$ vs T for the same magnetic fields, as indicated.

 https://doi.org/10.1038/s41567-024-02384-5

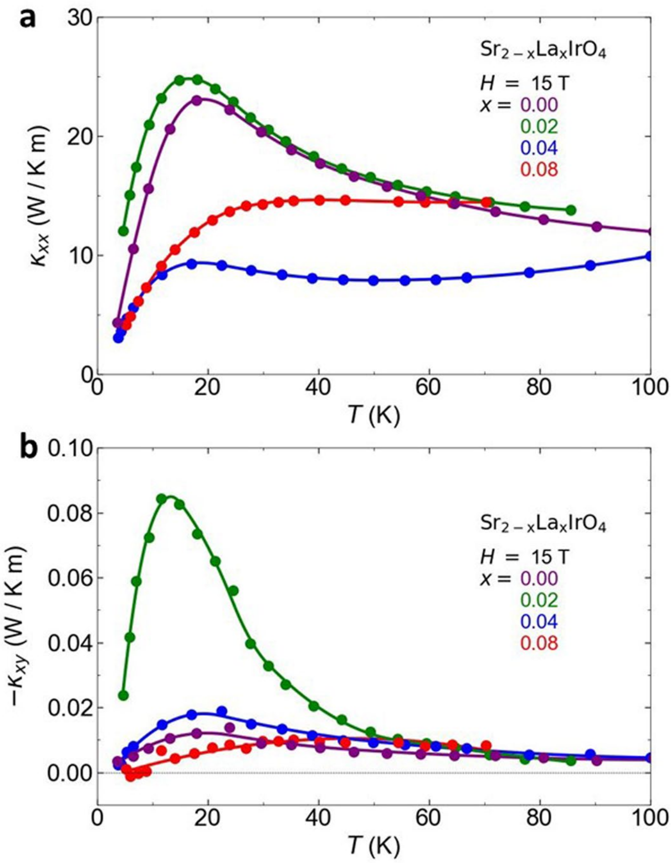

Extended Data Fig. 4 | Thermal conductivities in La-doped Sr_2IrO_4. **a)** Thermal conductivity κ_{xx} of $Sr_{2-x}La_xIrO_4$ for a heat current parallel to the IrO_2 planes (J // a // x) and a magnetic field of 15 T applied normal to the planes (H // c // z), plotted as κ_{xx} vs T, for dopings x as indicated. **b)** Thermal Hall conductivity κ_{xy} for the same samples, plotted as − κ_{xy} vs T (κ_{xy} is negative in all samples at all temperatures).

 https://doi.org/10.1038/s41567-024-02384-5

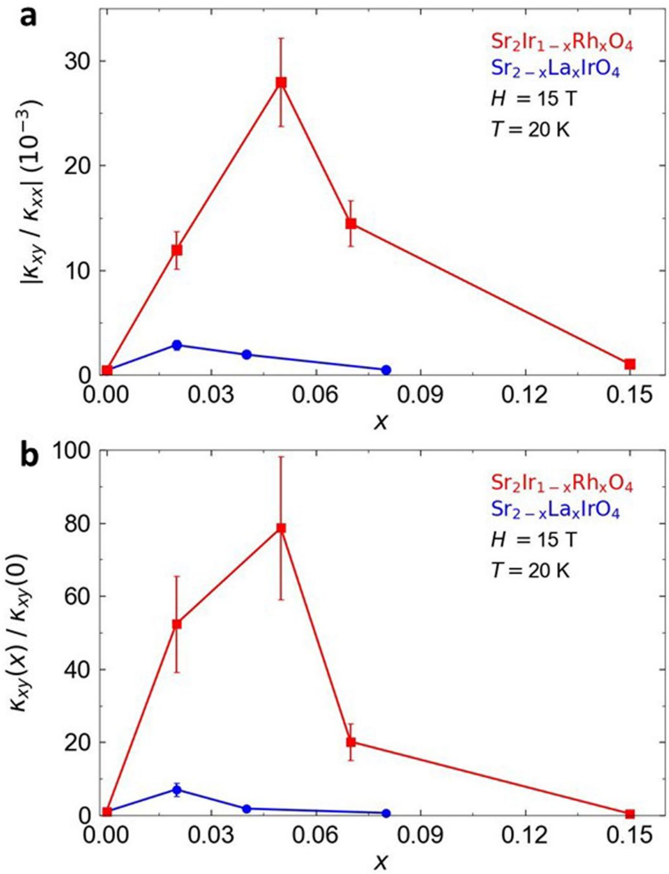

Extended Data Fig. 5 | Reproducibility of our two main findings. a) Evolution of the ratio $|\kappa_{xy}/\kappa_{xx}|$ in Sr_2IrO_4 with impurity concentration x, for both Rh doping (red squares) and La doping (blue circles), evaluated at T = 20 K and H = 15 T. Error bars are ± 15% (see Methods). **b)** Magnitude of the thermal Hall conductivity κ_{xy} in Sr_2IrO_4 vs x, evaluated at T = 20 K and H = 15 T, relative to its value at x = 0. We see that 3 separate samples of Rh-doped Sr_2IrO_4 – with x = 0.02, 0.05, 0.07 – demonstrate the main conclusion of our paper, namely that a low level of Rh impurities causes a huge enhancement of the thermal Hall angle, by a factor of at least 30 (or of the thermal Hall conductivity, by a factor of 20 or more) relative to x = 0. We also see that 3 separate samples of La-doped Sr_2IrO_4 – with x = 0.02, 0.04, 0.08 – demonstrate the second major conclusion of our paper, namely that La impurities cause a much smaller enhancement, by at least an order of magnitude compared to Rh doping. Having three separate samples that support each claim is a satisfactory level of reproducibility. Error bars are ± 25% (see Methods).